Elastoplastic Damaging Model for Adhesive Anchor Systems. I: Theoretical Formulation and Numerical Implementation

Antonino Spada[1]; Giuseppe Giambanco[2]; and Piervincenzo Rizzo[3]

Abstract: In this and in the companion paper, the mechanical response of adhesive anchor systems is theoretically and numerically predicted and experimentally observed. The theoretical prediction is on the basis of an elastoplastic damaging model formulated to predict the structural response associated with the development of a fracture in adhesive anchor systems. This part describes the analytical model developed in the framework of a thermodynamically consistent theory, which assumes adhesion where the structure is sound, and friction in correspondence with the fracture. Isotropic damage is considered. The model can predict the structural behavior at the interface between two surfaces of ductile, brittle, or quasi-brittle materials. The Helmholtz free energy is written to model the materials' hardening or softening. Isotropic damage is considered, and the possible effects of dilatancy are taken into account, including nonassociative flow rules. The formulation is implemented into the finite-element code FEAP. In the companion paper, the new model is adopted to predict the mechanical response to the pullout force of postinstalled rebar chemically bonded in concrete. The analytical model and the numerical implementation are experimentally validated by several pullout tests, which are monitored by using an acoustic-emission technique. **DOI: 10.1061/(ASCE)EM.1943-7889.0000287.**

CE Database subject headings: Elastoplasticity; Damage; Pullout; Interfaces; Finite element method; Anchors; Implementation.

Author keywords: Elastoplasticity; Damage; Pullout test; Interface; Finite elements; FEAP; Acoustic emission.

Introduction

Epoxy adhesive anchor systems are widely used in civil engineering to, for instance, anchor both threaded rods and reinforce bar into hardened concrete. Common applications include bridge widening, structure-mounted signs, luminaries and light poles, concrete repair and rehabilitation, and tunneling finishing.

Anchors can be divided into two general groups: cast-in-place and postinstalled. A typical cast-in-place anchor can be a rebar in concrete with or without protective coating. A postinstalled anchor is a rebar installed in a hole and then bonded with a chemical or nonchemical agent. Many chemical agents are available, and they usually come in two components that activate a chemical reaction once they are mixed together. Nonchemical agents like mortar or cementitious grout are less expensive, but they require a larger hole to ease the installation. Bonded anchors utilizing nonchemical agents are often called grouted anchors and are widely adopted in tunnel and mining engineering (Cook 1993). The interaction between bolt and rock mass was studied by Peng and Tang (1984), Mark et al. (2002), Cai et al. (2004), and Sakurai (2010).

The use of chemically bonded anchors is increasing because of the development of strong chemical agents such as polyester, vinylester, and epoxy. In concrete structures, chemically bonded anchors are used to cast secondary floor slabs, close temporary openings, cast new wall, expand existing buildings, connect columns with the foundation, and connect cantilevering elements such as balconies, stairways, and landing slabs with existing structures. In all of these examples, the use of chemically bonded anchors is preferred to the cast-in-place method, and in some cases, it represents the only viable way to proceed. However, the use of such anchors requires the full comprehension of the stress distribution, failure modes, and main factors that influence the strength of these systems.

It is known that cast-in-place structures are structurally stronger than postinstalled systems. Castro (1996) studied the influence of coatings on bar-concrete bond. By using strut tests, he demonstrated that the bond strength of an epoxy-coated rebar system is 8.6% weaker than a cast-in-place bar-concrete system. Gustafson (1988) reported the outcomes from pullout tests conducted on cast-in-place concrete-rebar systems and epoxy-coated rebars embedded in concrete. It was found that the bond strength of coated rebars is 66% of the cast-in-place systems.

A pullout test is a standard experimental procedure to evaluate the bond strength between steel-concrete or steel-adhesive-concrete interfaces. Although several analytical, numerical, and experimental studies were conducted on steel-concrete interaction, the same cannot be said about the steel-adhesive-concrete system. Pullout tests were conducted on rebar embedded in concrete to delve into the splitting phenomenon, the influence of the ribs, and the bond length on the final resistance. Ghandehari et al. (1999, 2000) evaluated the stages of the splitting of concrete in the absence of confining effects other than the concrete cover. They assessed the

[1]Postdoctoral Scholar, Dept. of Civil, Environmental, and Aerospace Engineering, Univ. of Palermo, Viale delle Scienze—Ed. 8–90128, Palermo, Italy.

[2]Professor, Dept. of Civil, Environmental, and Aerospace Engineering, Univ. of Palermo, Viale delle Scienze—Ed. 8–90128, Palermo, Italy.

[3]Assistant Professor, Laboratory for Nondestructive Evaluation and Structural Health Monitoring Studies, Dept. of Civil and Environmental Engineering, Univ. of Pittsburgh, 942 Benedum Hall, 3700 O'Hara Street, Pittsburgh, PA 15261 (corresponding author). E-mail: pir3@pitt.edu

Note. This manuscript was submitted on August 13, 2010; approved on June 18, 2011; published online on June 21, 2011. Discussion period open until May 1, 2012; separate discussions must be submitted for individual papers. This paper is part of the ***Journal of Engineering Mechanics***, Vol. 137, No. 12, December 1, 2011. ©ASCE, ISSN 0733-9399/2011/12-854–861/$25.00.

relationship between stress and relative displacement at the interface for splitting failure. Nonlinear fracture mechanics was used to model the bond-splitting failure. Hageman et al. (1986) conducted monotonic pullout tension tests, and cyclic tests of full-scale reinforced concrete panels to validate a model (Murakami and Hegemier 1986) for a steel-concrete bond. Yeih et al. (1997) studied the interface properties between rebar and concrete. Gambarova et al. (1994) proposed an elastocohesive model on the basis of crack cohesion, concrete failure in plane stresses, outer-pressure effects, and minimum crack number. Another analytical model proposed by Wang and Liu (2003) assumed a smeared cracking and a strain-softening model for bond strength. Finally, Qian and Li (2009) studied the influence of material ductility on the anchor pullout performance by replacing normal concrete with engineered cementitious composites that strain hardens to several percent tensile-strain capacity.

Efforts to understand the behavior of chemically bonded anchors were made by Cook (1993) and Sakla and Ashour (2005). Cook (1993) conducted a comprehensive investigation on the following existing mathematical models to predict the possible failures of the system: concrete cone failure model, uniform and elastic model for bond failure, and combined cone-bond failure model. The results of 144 pullout tests using 16 different adhesives, three different bond lengths, and differences between confined or not-confined concrete were reported. Sakla and Ashour (2005) determined that the tensile capacity of cohesive anchors is directly proportional to the anchor diameter and the embedment depth.

McVay et al. (1996) reported on the state-of-the-art of the elastoplastic finite-element simulations of pullout of postinstalled anchors. They also compared numerical simulations and experimental results. Comparisons between analytical and experimental data were also presented by Obata et al. (1998), who proposed a method to estimate the cone failure strength using the theory of linear fracture mechanics implemented in the finite-element code ABAQUS.

In this paper, an analytical elastoplastic damaging interface model is presented. The model is specifically applied to predict the mechanical response to the pullout force of a postinstalled rebar embedded in hardened concrete cylinders by using polyester resin. The model is presented in the framework of a thermodynamically consistent theory, and has been implemented in the finite-element code FEAP. Two different approaches are proposed, namely, a simplified micromodeling and a detailed micromodeling. In the first approach, the polyester resin and the two physical interfaces rebar-resin and resin-concrete are lumped together. A unique interface element is introduced between the rebar and the concrete. In the detailed micromodeling, one interface element is introduced between the rebar and the resin, and a second interface element is introduced between the resin and the concrete. Rebar, resin, and concrete are assumed to be linear elastic. The nonlinear behavior is concentrated in correspondence of the interfaces.

The model is numerically and experimentally validated. The experimental validation is accompanied by a nondestructive evaluation approach on the basis of the acoustic emission (AE) technique. The results of such a validation are presented in the companion paper. The main contribution of the present study is twofold. The elastoplastic damaging model recently introduced by Spada et al. (2009) is, for the first time, applied to postinstalled chemically bonded anchors. The use of AE to monitor the onset and propagation of cracks in such structures and to validate the analytical model represents another element of novelty.

This paper is organized as follows. First, the main aspects of the analytical model and its finite-element implementation are provided. Then, an overview of the pullout test is given for the sake of completeness. The companion paper will provide an overview of the general concepts of the AE techniques. Finally, the results of the numerical implementation and the experimental validation are presented.

Theoretical Model

Analytical Formulation

In the Euclidean space R^3, referred to as the orthonormal frame $(O, \mathbf{i}_1, \mathbf{i}_2, \mathbf{i}_3)$, consider a body formed by two adherents Ω^+ and Ω^- connected by an adhesive joint Ω through the two surfaces Σ^+ and Σ^- [Fig. 1(a)]. Assume the thickness h of the joint, small when compared with the characteristic dimensions of the bonded assembly. Therefore, the joint Ω^j and the surfaces Σ^+ and Σ^- can be regarded as a contact layer or interface model Σ with a constant thickness h.

To characterize the kinematics at the interface (opening, sliding, dilatancy) the displacement discontinuity vector $[\mathbf{u}]$ can be defined as

$$[\mathbf{u}] = \mathbf{u}^+ - \mathbf{u}^- \tag{1}$$

If a local Cartesian reference system $(O, \mathbf{e}_1, \mathbf{e}_2, \mathbf{e}_3)$ is considered [Fig. 1(b)], it is possible to write

$$[\mathbf{u}] = [u_1]\mathbf{e}_1 + [u_2]\mathbf{e}_2 + [w]\mathbf{e}_3 \tag{2}$$

where $[u_1]$ and $[u_2]$ = tangential displacement discontinuities; and $[w]$ = normal displacement discontinuity. Similarly, a stress discontinuity vector $[\sigma]$ can be defined as

$$[\sigma] = \sigma^+ - \sigma^- = [\tau_1]\mathbf{e}_1 + [\tau_2]\mathbf{e}_2 + [\sigma]\mathbf{e}_3 \tag{3}$$

where $[\tau_1]$ and $[\tau_2]$ = tangential stress discontinuities; and $[\sigma]$ = normal stress discontinuity.

Consider now a representative volume element (RVE) of thickness h and infinitesimal middle-plane area S, as shown in Fig. 2. It is assumed that (1) the traction components are continuous,

$$[\tau_1] = 0, \qquad [\tau_2] = 0, \qquad [\sigma] = 0 \tag{4}$$

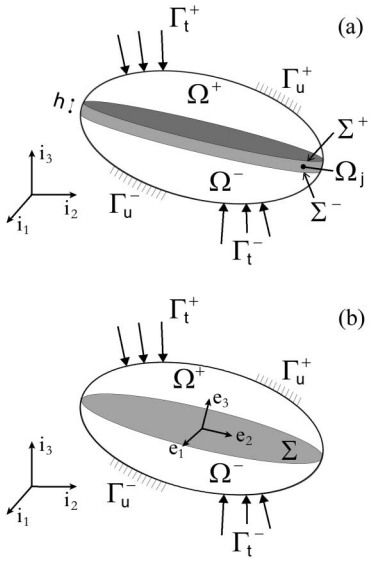

Fig. 1. (a) Interface mechanical scheme; (b) mechanical scheme of a third body interposed between two adherents

J. Eng. Mech. 2011.137:854-861.

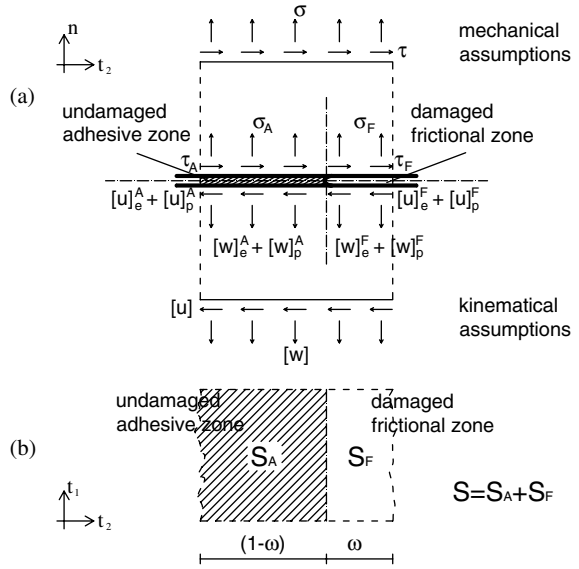

Fig. 2. Representative volume element with mechanical and kinematical assumptions: (a) front view, (b) plane view (Spada et al. 2009, with permission)

and (2) the strain components along the thickness h are uniform,

$$[\gamma_1] = \frac{[u_1]}{h}, \qquad [\gamma_2] = \frac{[u_2]}{h}, \qquad [\varepsilon] = \frac{[w]}{h} \tag{5}$$

To account for the presence of defects such as voids and fractures within the material, the RVE is divided into two parts, the undamaged adhesive or cohesive part, and the damaged frictional part. In the first part, an elastoplastic behavior associated with cohesive forces is assumed. In the damaged frictional part, an elastoplastic response associated with the sliding frictional effects because of the occurrence of damage is assumed. The two parts are treated like two uncoupled phases, and each phase is studied by using proper constitutive relationships. The damage parameter ω is introduced as the ratio between the damaged area S_F and the total area S of the RVE,

$$\omega = \frac{S_F}{S} \tag{6}$$

The extreme values $\omega = 0$ and $\omega = 1$ identify a pristine and a totally damaged state, respectively; damage is considered isotropic. According to the theory of plasticity (Maugin 1992; Lemaitre and Chaboche 1990), the observable total strains ε and displacement discontinuities $[\mathbf{u}]$ are the sum of the elastic (e) and plastic (p) internal components,

$$\varepsilon^{A,F} = \varepsilon_e^{A,F} + \varepsilon_p^{A,F} \quad \text{or} \quad [\mathbf{u}]^{A,F} = [\mathbf{u}]_e^{A,F} + [\mathbf{u}]_p^{A,F} \tag{7}$$

where the apexes A and F = adhesive and frictional phases, respectively.

By replacing Eq. (5) in the classic elastic stress-strain relationships and adopting the notation in Eq. (7), the following relationships between stresses and elastic displacement discontinuities are derived:

$$\sigma^A = \mathbf{E}^A \varepsilon_e^A = \mathbf{E}^A \frac{[\mathbf{u}]_e^A}{h} = \mathbf{K}^A [\mathbf{u}]_e^A \tag{8}$$

$$\sigma^F = \mathbf{E}^F \varepsilon_e^F = \mathbf{E}^F \frac{[\mathbf{u}]_e^F}{h} = \mathbf{K}^F [\mathbf{u}]_e^F \tag{9}$$

In Eqs. (8) and (9), $\mathbf{E}^A$ and $\mathbf{E}^F$ = elastic matrices of the adhesive and damaged phases, respectively, and $\mathbf{K}^A = \mathbf{E}^A/h$ and $\mathbf{K}^F = \mathbf{E}^F/h$ are the correspondent interface elastic-stiffness matrices.

Imposing the equilibrium of the RVE, the total stress σ at the interface can be written as

$$\sigma = (1-\omega)\sigma^A + \omega\sigma^F \tag{10}$$

To find the state laws and the flow rules to describe a mechanical process, the thermodynamical approach is used. For small displacements, and in the case of constant and uniform temperature, by combining the first and the second principles of thermodynamics, the following Clausius-Duhem inequality is imposed:

$$D = \sigma^T [\dot{\mathbf{u}}] - \dot{\Psi} \geq 0 \tag{11}$$

where D = scalar function known as intrinsic dissipation; the dot = time derivative; and the function Ψ = specific Helmholtz free potential energy. In the mesoscopic model adopted in this study, Ψ is defined as

$$\Psi([\mathbf{u}]_e^A, [\mathbf{u}]_e^F, \xi_p, \xi_d, \omega) = (1-\omega)\Psi^A([\mathbf{u}]_e^A, \xi_p) + \omega\Psi^F([\mathbf{u}]_e^F) + \Psi^{AF}(\xi_d) \tag{12}$$

where ξ_p and ξ_d = vectors of internal plastic variables and internal damage variables, respectively. Eq. (12) can be regarded as a weighted average of the free potential energies of the two parts of the RVE, plus a specific energy controlling the evolution of damage.

Because the Helmholtz free energy is a potential, the state laws that define the mechanical variables can be obtained by deriving Eq. (12) with respect to the associated kinematic variables. Therefore, the following set of mechanical variables can be defined:

$$\sigma^A = \frac{\partial\Psi}{\partial[\mathbf{u}]_e^A}, \qquad \sigma^F = \frac{\partial\Psi}{\partial[\mathbf{u}]_e^F}, \qquad \chi_p = \frac{\partial\Psi}{\partial\xi_p}, \qquad \chi_d = \frac{\partial\Psi}{\partial\xi_d}, \qquad \varsigma = \frac{\partial\Psi}{\partial\omega} \tag{13}$$

where χ_p, χ_d, and ς are usually referred to as the thermodynamic forces associated with the internal variables ξ_p, ξ_d, and ω, respectively.

Because the onset and growth of plasticity and damage can be considered an evolutionary mechanical process and the dissipation has a nonnegative maximum, the theorem of maximum dissipation (Lemaitre and Chaboche 1990) must be applied to obtain the flow rules of the kinematical variables. According to this theorem, the maximum value of the intrinsic dissipation D must be found. The maximum of the function D can be found by the Lagrangian method. In this approach, a Lagrangian function $L()$ is defined as

$$L(\sigma^A, \sigma^F, \chi_p, \chi_d, \varsigma) = D - \sum_i \dot{\lambda}_i \phi i \tag{14}$$

where $\dot{\lambda}_i$ = Lagrangian multipliers; and ϕ^i = constraint functions, which define the activation of a particular mechanism. The variables $\dot{\lambda}_i$ and ϕ^i must satisfy the following complementary conditions (Kuhn-Tucker relations):

$$\phi^i \leq 0, \qquad \dot{\lambda}_i \geq 0, \qquad \dot{\lambda}_i \phi^i = 0, \qquad \dot{\lambda}_i \dot{\phi}^i = 0 \tag{15}$$

Finally, the flow rules are calculated by solving the system obtained deriving the Lagrangian function with respect to each

J. Eng. Mech. 2011.137:854-861.

mechanical variable and imposing it:

$$\frac{\partial L}{\partial \sigma^A} = \mathbf{0}, \quad \frac{\partial L}{\partial \sigma^F} = \mathbf{0}, \quad \frac{\partial L}{\partial \chi_p} = \mathbf{0}, \quad \frac{\partial L}{\partial \chi_d} = 0, \quad \frac{\partial L}{\partial \varsigma} = 0 \tag{16}$$

In this paper, a bidimensional model is used, and the specific Helmholtz free potential energies used in this paper are

$$\Psi^A([\mathbf{u}]_e^A, \xi_p) = \frac{1}{2}[\mathbf{u}]_e^{AT}\mathbf{K}^A[\mathbf{u}]_e^A + \frac{1}{2}\xi_p^T\mathbf{H}_p\xi_p \tag{17a}$$

$$\Psi^F([\mathbf{u}]_e^F) = \frac{1}{2}[\mathbf{u}]_e^{FT}\mathbf{K}^F[\mathbf{u}]_e^F \tag{17b}$$

$$\Psi^{AF}(\xi_d) = h_d\left[\sum_{i=0}^{p-1}\frac{p!}{i!}\ln^i c + \ln^p c - (1-\xi_d)\sum_{i=0}^{p}\frac{p!}{i!}\ln^i\frac{c}{1-\xi_d}\right] \tag{17c}$$

with

$$[\mathbf{u}] = [\,[w] \quad [u]\,] \tag{18a}$$

$$\mathbf{H}_p = \begin{bmatrix} \left(\frac{\sigma_0}{c_0}\right)^2 h_p & \left(\frac{\sigma_0}{c_0}\right)h_p \\ \left(\frac{\sigma_0}{c_0}\right)h_p & h_p \end{bmatrix} \tag{18b}$$

The values of h_d, c, and p are empirical constants. The model's hardening parameter h_p is related to the model's damage threshold ς_0 through the following relationship:

$$\varsigma_0 = h_d \ln^p c \tag{19}$$

Eq. (17*c*) is the same proposed by Comi and Perego (2004). In this study, the elastic matrices $\mathbf{E}^A$ and $\mathbf{E}^F$ are given by the following:

$$\mathbf{E}^A = \begin{bmatrix} E_t\langle \mathrm{Sign}([w]_e^A)\rangle + E_c\langle -\mathrm{Sign}([w]_e^A)\rangle & 0 \\ 0 & G^A \end{bmatrix} \tag{20a}$$

$$\mathbf{E}^F = \begin{bmatrix} E_c & 0 \\ 0 & G^F \end{bmatrix} \tag{20b}$$

where E_t and E_c = longitudinal elastic moduli in tensile and compression stress, respectively; and G^A and G^F = tangential elastic moduli of the two phases of the interface. The symbol $\langle\circ\rangle$ denotes the MacAulay operator defined as $\langle\circ\rangle = [(\circ) + |\circ|]/2$.

Four constraint functions are also considered:

$$\phi_p^A = |\tau^A| + \sigma^A\tan(\varphi_A) - c_0 - \chi_{p2}(\xi_p) \tag{21a}$$

$$\phi_p^T = \sigma^A - \sigma_0 - \chi_{p1}(\xi_p) \tag{21b}$$

$$\phi_p^F = |\tau^F| + \sigma^F\tan(\varphi_F) \tag{21c}$$

$$\phi_d = \varsigma_A^+ - \chi_d \tag{21d}$$

where φ_A and φ_F = internal frictional angles of the undamaged and damaged phases, respectively; c_0 and σ_0 = initial cohesion and the tensile threshold, respectively; and χ_{p1} and χ_{p2} = components of the vector χ_p. A schematic representation of all these domains is given in Fig. 3, in which the different zones are identified by the limit functions.

In the nonassociative case, the plastic potentials related to the Mohr-Coulomb limit conditions [Eqs. (21*a*) and (21*c*)] can be written as

$$\Gamma_p^A = |\tau^A| + \sigma^A\tan(\mu_A) - r \tag{22a}$$

$$\Gamma_p^F = |\tau^F| + \sigma^F\tan(\mu_F) - s \tag{22b}$$

where μ_A and μ_F = dilatancy angles; and r and s = two arbitrary constants chosen to satisfy Eq. (22). Finally, the following condition on parameters

$$\frac{K_t^A}{K_t^F} \le \frac{\tan\varphi_A}{\tan\varphi_F} \tag{23}$$

is considered.

Numerical Implementation

The analytical model proposed in this paper was implemented in a finite-element subroutine as a novel part of an existing user element (Giambanco et al. 2001), and interfaced with the open-source finite-element code FEAP (Taylor 2005a, b). The user element is a bidimensional interface element of quadrilateral shape. The shape is defined by four or six nodes. The Gauss points or the Lobatto points can be selected as integration points. To implement the analytical formulation, a time-discretization of the constitutive model on the basis of the implicit backward-Euler difference scheme (Simo and Ju 1987) was used. The discrete equations are considered in the framework of a two-step algorithm that splits the solution problem in an elastic trial predictor stage and a plastic and/or damaging corrector stage. Neglecting any plastic or damaging mechanism inside the time step $[t_n, t_{n+1}]$, the elastic predictor stage, leads to the following results:

$$\text{predictor}\left\|\begin{array}{l} [\mathbf{u}]_{p,n+1}^{A,\text{trial}} = [\mathbf{u}]_{p,n}^A \\ [\mathbf{u}]_{p,n+1}^{F,\text{trial}} = [\mathbf{u}]_{p,n}^F \\ \xi_{p,n+1}^{\text{trial}} = \xi_p \\ \xi_{d,n+1}^{\text{trial}} = \xi_{d,n} \\ \omega_{n+1}^{\text{trial}} = \omega_n \end{array}\right. \Rightarrow \left\|\begin{array}{l} [\mathbf{u}]_{e,n+1}^{A,\text{trial}} = [\mathbf{u}]_{n+1} - [\mathbf{u}]_{p,n+1}^{A,\text{trial}} \\ [\mathbf{u}]_{e,n+1}^{F,\text{trial}} = [\mathbf{u}]_{n+1} - [\mathbf{u}]_{p,n+1}^{F,\text{trial}} \\ \sigma_{n+1}^{A,\text{trial}} = \mathbf{K}^A[\mathbf{u}]_{e,n+1}^{A,\text{trial}} \\ \sigma_{n+1}^{F,\text{trial}} = \mathbf{K}^F[\mathbf{u}]_{e,n+1}^{F,\text{trial}} \end{array}\right. \tag{24}$$

Once the trial quantities are known, Eq. (24) is substituted into the plastic and damaging limit functions (Eq. (22)) rewritten at time t_{n+1}. If the loading/unloading conditions given in Eq. (15), also written in a discrete way and calculated at time t_{n+1}, are not satisfied, a corrector phase is needed. In this case, all the activated functions are set to be zero, whereas the relative plastic or damaging multipliers have to be positive. These conditions imply that a system of nonlinear functions has to be solved for the plastic or damaging multipliers' unknowns. A Newton-Raphson iterative procedure is used to solve this system numerically. Finally, all the kinematical and mechanical variables are updated, the nodal displacements and stresses are taken out from the subroutine, and the program moves to another integration point or to the subsequent time step.

Recently, Spada et al. (2009) validated the numerical implementation by studying three structural problems, namely, a concrete beam subjected to a 4-points bending loading, a masonry wall loaded in shear, and a masonry vault subjected to a point load. The numerical results were compared to results available in literature.

J. Eng. Mech. 2011.137:854-861.

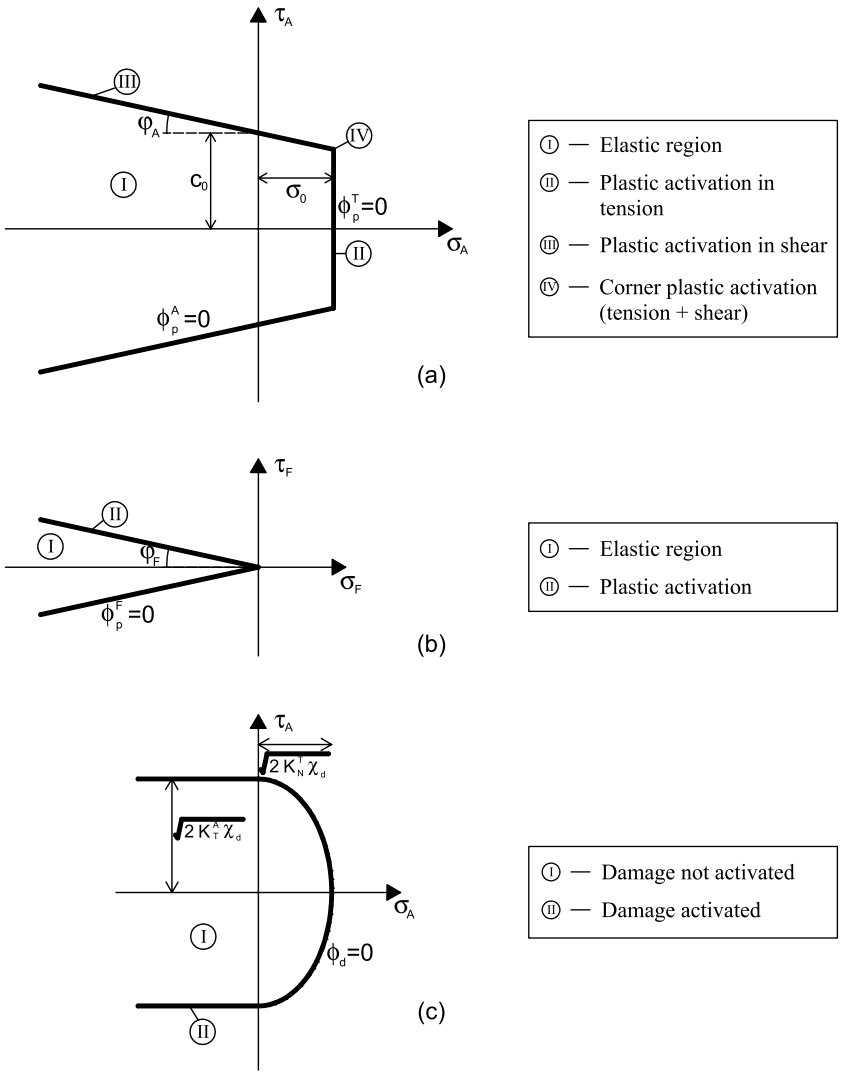

Fig. 3. (a) Plastic adhesive, (b) plastic frictional, and (c) damage activations domains (Spada et al. 2009, with permission)

Pullout Test: Background and Failure Modes

The pullout test measures the force required to pull an embedded bar from a concrete specimen or a structure (Malhotra and Carino 2004).

While in the cast-in-place anchors, the load is transferred into the concrete at the anchor head; in the case of adhesive anchors, the load is transferred from the steel through the adhesive layer along the entire bonded surface. The bond at the interface consists of three mechanisms: adhesion, friction, and mechanical interlock.

In perfect conditions, the bond between the steel and the adhesive medium or concrete is because of chemical adhesion. Once the chemical connections fail and relative displacements occur between the two surfaces, the friction forces dominate [Fig. 4(a)]. If debonding takes place around the rebar surface, the ribs govern the stress-deformation behavior. When the resin between the ribs is subjected to a shear force, its deformation creates a bar-resin mechanical interlock dependent on the ribs' geometry [Fig. 4(b)]. The inclined shape of the ribs is subjected to a force N orthogonal to the ribs' surface, which turns into a reaction R acting on the resin or concrete [Fig. 4(c)].

When the rebar is cast-in-place without coating at the early stages of a pullout test, inclined cracks (theoretically at 45°) start to appear because of pure shear stress in the concrete, which yields tensile and compressive stresses along the principal directions. When the load increases, the horizontal component R_0 of the reaction force R represents an increasing radial force that, for large slip

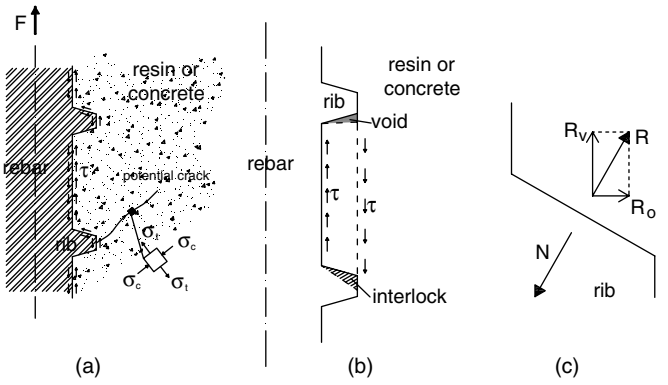

Fig. 4. (a) Stress distribution and (b) deformations at the interface rebar-resin (or concrete) during the pullout test; (c) forces acting on the ribs

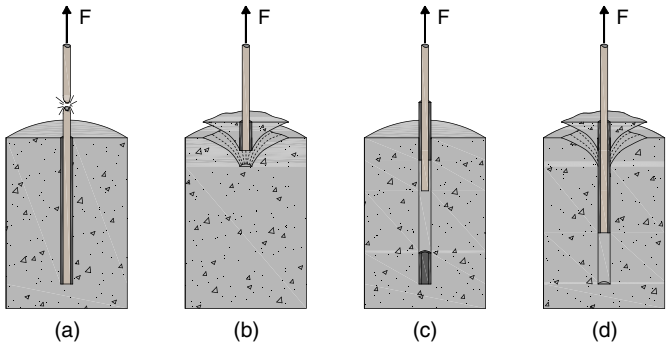

Fig. 5. Failure modes during a pullout test for unconfined concrete: (a) steel failure, (b) concrete cone failure, (c) bond failure, and (d) combined cone-bond failure (Rizzo et al. 2010, with permission)

values, promotes the development of longitudinal cracks. This mode of failure is usually referred to as splitting failure.

When rebars are chemically bonded, the higher tensile limit stress leads to different possible types of failure modes, depending on the boundary and anchoring conditions. The typical failure modes are shown in Fig. 5 and can be classified as the following (Cook 1993; Sakla and Ashour 2005):

1. Anchor steel failure characterized by yielding or fracture of the steel;
2. Concrete cone failure occurring when the embedment depth is less than 50 mm and the concrete is unconfined;
3. Bond failure at the bar-resin or resin-concrete interfaces; and
4. Combined cone-bond failure usually in unconfined concrete and embedment depth greater than 50–100 mm.

Several variables influence the tensile pullout strength of bonded rebars, namely, bonding agents, concrete, steel, surface roughness, temperature, and loading gradients (Cook 1993; Sakla and Ashour 2005).

Numerical Implementation of Pullout Test

The analytical formulation discussed in the section "Theoretical Model" was numerically implemented in FEAP to predict the structural response of the system schematized in Fig. 6 subjected to pullout. Both the simplified micromodeling and the detailed micromodeling were used to show their applicability to this particular case and to establish a priority in the choice of one of these two methods.

In the first approach, the resin and the two physical interfaces rebar-resin and resin-concrete were lumped together and substituted by a single interface layer of zero thickness. Thus, only three materials are needed for the analysis: steel, interface, and concrete. Because of the geometric properties, the system was considered axisymmetric, which reduced the number of finite elements and the computational effort. Bidimensional elements were used in FEAP to model the solid elements. Also, loading nodal forces were computed for one radiant segment in the circumferential direction (Taylor 2005a).

The rebar was assumed to be smooth and elastoplastic, with an elastic tensile limit equal to 418 MPa. The scheme of the chemically bonded anchor and its finite-element mesh representation studied in this paper are shown in Figs. 6(a) and 6(b), respectively. Table 1 summarizes the geometric properties of the mesh and the material properties. Each element has rectangular shape.

Three Lobatto points were selected as integration points for each interface element. The parameters used for the interface elements were chosen on the basis of the experimental results that will be discussed subsequently. The boundary condition included restraint of vertical displacements on top of the concrete. This restraint, together with the appropriate bond length, allows for shear pullout failure only and avoids the concrete cone failure. Other restraints were imposed on the vertical displacements at the bottom of the cylinder, and radial and vertical displacements of node A, indicated in Fig. 6(b).

In the detailed micromodel, all physical elements were considered with their real geometry. Therefore, five different materials were considered: steel, rebar-resin interface, resin, resin-concrete interface, and concrete. The number of elements and the mechanical characteristics of the steel and concrete elements are the same as in the simplified micromodel. Owing to the different mechanical characteristics of the materials at the interface, the analytical parameters utilized to describe the mechanical properties should differ. Such parameters can be determined only on the basis of

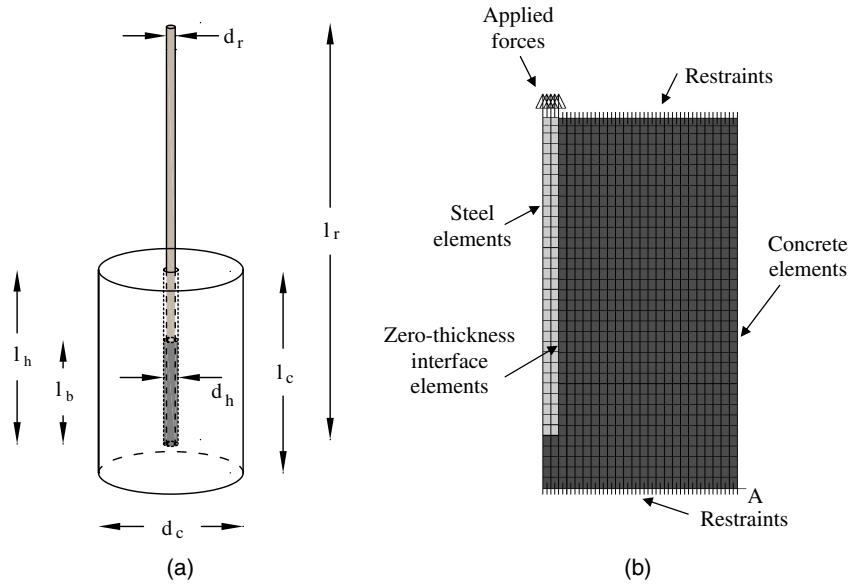

Fig. 6. (a) Detail on the system's geometric parameters; (b) simplified micromodel: finite-element mesh

J. Eng. Mech. 2011.137:854-861.

Table 1. Finite-Element Model: Mechanical and Geometrical Properties of the Elements

	Steel	Resin[a]	Concrete	
			Below the rebar	Beside the rebar
Number of rectangular elements	62	not available[b]	120	682
Element size (mm × mm)	5.2 × 10.0	4.7 × 10.0	5.2 × 10.8	5.3 × 10.0
Number of nodes per element	8	8	8	
Young's modulus (MPa)	210,000	6,500	21,197	
Poisson's ratio	0.3	0.2	0.16	

[a]Only for the detailed micromodel.
[b]The number of elements changes according with the bonding length.

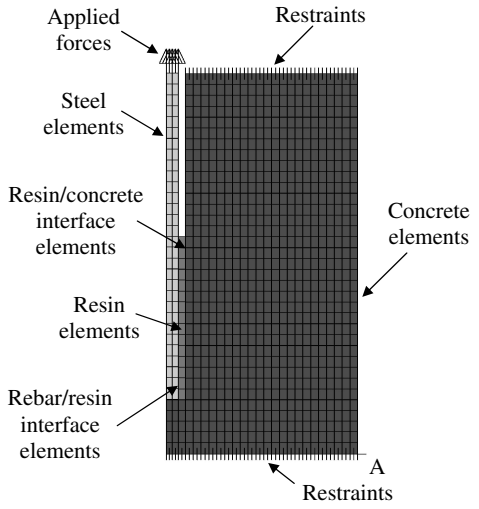

Fig. 7. Detailed micromodel: finite-element mesh

experimental results. A schematic view of the mesh used for the second approach is shown in Fig. 7.

The detailed formulation simulates the presence of both interfaces, i.e., the two contact surfaces concrete-resin and resin-rebar. These interfaces capture the mechanical nonlinearities that take place at the bonding level thanks to the use of a greater (with respect to the simplified model) number of calibration parameters. Moreover, the detailed model accurately captures the sequence of events during a pullout test. For example, rebar debonding can take place at the concrete-resin interface level or at the resin-rebar one [Fig. 5(c)]. Either event is captured, provided the parameters are properly calibrated. The accuracy of the detailed model comes, however, at the expense of the large number of parameters that need to be calibrated. Moreover, this calibration is accurate only if certain mechanisms of plasticity and/or damage are experimentally activated at each interface. When this condition is not observed experimentally, the model's parameters are estimated to prevent the numerical occurrence of the mechanism of activation. This approach might degrade the agreement between the results of the numerical model from the observations from the experimental result, especially for complex structural elements such as masonry. Finally, the detailed model requires larger computational effort owing to the increased number of finite elements involved in the analysis and the larger number of parameters to calibrate.

The simplified model overcomes all the drawbacks associated with the detailed model. In the simplified model, the epoxy and the two interfaces that separate the epoxy to the rebar and the concrete are considered as a single interface layer of zero thickness. As demonstrated in the companion paper (part II), this model provides qualitative responses that are in good agreement with the experimental results and close to the values obtained with the numerical detailed model.

All numerical simulations were carried out using the arclength solution (Taylor 2005a, b). This is a continuation method on the basis of maintaining a constant length of a specified load-displacement path. This solution method permits overcoming problems associated with the snap-back phenomena, which occurs especially when a fracture is developing and a redistribution of stresses takes place. No snap-back phenomena are expected in this study because of the symmetry of the system. In fact, interface elements are frequently subjected to shear forces because of the imposition of tangential displacements. Because these displacements are the same for each interface element, their response is identical. This means that a uniform stress can be found along the bond length at any instant of the simulation.

Conclusions

In this paper, a new analytical elastoplastic damaging interface model has been applied to study experimental pullout tests on concrete reinforced with chemically bonded anchors. The interface model has been presented in the framework of a thermodynamically consistent theory, and has been implemented in a finite-element subroutine in the open source code FEAP. Two different types of numerical models have been used: a simplified micromodel and a detailed micromodel. Both models have given good results with respect to the experimental data, but the simplified model can be preferred because of its simpler implementation and lower computational time requirement.

The theoretical model and its numerical implementation will be validated using the testing program discussed in the companion paper.

Acknowledgments

The first author conducted part of this research while visiting the University of Pittsburgh under a Study Abroad Fellowship of the University of Palermo's School of Engineering. The support of the University of Pittsburgh through startup funds available to the corresponding author is also acknowledged.

References

Cai, Y., Esaki, T., and Jiang, Y. (2004). "A rock bolt and rock mass interaction model." *Int. J. Rock Mech. Min. Sci. Geomech. Abstr.*, 41(7), 1055–1067.

Castro, P. F. (1996). "Influence of coatings on bar-concrete bond." *J. Mater. Civ. Eng.*, 8(4), 212–214.

Comi, C., and Perego, U. (2004). "Criteria for mesh refinement in nonlocal damage finite element analyses." *Eur. J. Mech. A. Solids*, 23(4), 615–632.
Cook, R. A. (1993). "Behavior of chemically bonded anchors." *J. Struct. Eng.*, 119(9), 2744–2762.
Gambarova, P. G., Rosati, G. P., and Schumm, C. (1994). "An elasto-cohesive model for steel-concrete bond." *Fracture and damage in quasi-brittle structures: Experiment, modelling and computation*, Z. P. Bazant, Z. Bittnar, M. Jirasek, and J. Mazars, eds., E & FN Spon, London, 557–566.
Ghandehari, M., Krishnaswamy, S., and Shah, S. (1999). "Technique for evaluating kinematics between rebar and concrete." *J. Eng. Mech.*, 125(2), 234–241.
Ghandehari, M., Krishnaswamy, S., and Shah, S. (2000). "Bond induced longitudinal fracture in reinforced concrete." *J. Appl. Mech.*, 67(4), 740–748.
Giambanco, G., Rizzo, S., and Spallino, R. (2001). "Numerical analysis of masonry structures via interface models." *Comput. Methods Appl. Mech. Eng.*, 190(49–50), 6493–6511.
Gustafson, D. P. (1988). "Epoxy update." *J. Civ. Eng.*, 58(10), 38–41.
Hageman, L. J., Murakami, H., and Hegemier, G. A. (1986). "On simulating steel-concrete interaction in reinforced concrete part II: Validation studies." *Mech. Mater.*, 5(2), 171–185.
Lemaitre, J., and Chaboche, J. L. (1990). *Mechanics of solids materials*, Cambridge Univ. Press, Cambridge, UK.
Malhotra, V. M., and Carino, N. J. (2004). *Handbook on nondestructive testing of concrete*, 2nd Ed., CRC Press, Boca Raton, FL.
Mark, C., Compton, C. S., Oyler, D. C., and Dolinar, D. R. (2002). "Anchorage pull testing for fully grouted roof bolts." *Proc., 21st Int. Conf. Ground Control in Mining*, West Virginia Univ., Morgantown, WV, 105–113, ⟨http://cdc.ba0.biz/niosh/mining/pubs/pdfs/aptff.pdf⟩.
Maugin, G. A. (1992). *The thermomechanics of plasticity and fracture*, Cambridge Univ. Press, Cambridge, UK.
McVay, M., Cook, R. A., and Krishnamurthy, K. (1996). "Pullout simulation of post-installed chemically bonded anchors." *J. Struct. Eng.*, 122(9), 1016–1024.
Murakami, H., and Hegemier, G. A. (1986). "On simulating steel-concrete interaction in reinforced concrete part I: Theoretical development." *Mech. Mater.*, 5(2), 171–185.
Obata, M., Inoue, M., and Goto, Y. (1998). "The failure mechanism and the pullout strength of a bond-type anchor near a free edge." *Mech. Mater.*, 28(1–4), 113–122.
Peng, S. S., and Tang, D. H. Y. (1984). "Roof bolting in underground mining: A state-of-the-art review." *Geotech. Geol. Eng.*, 2(1), 1–42.
Qian, S., and Li, V. C. (2009). "Influence of concrete material ductility on headed anchor pullout performance." *ACI Mater. J.*, 106(1), 72–81.
Rizzo, P., Spada, A., Degala, S., and Giambanco, G. (2010). "Acoustic emission monitoring of chemically bonded anchors." *J. Nondestruct. Eval.*, 29(1), 49–61.
Sakla, S. S. S., and Ashour, A. F. (2005). "Prediction of tensile capacity of single adhesive anchors using neural networks." *Comput. Struct.*, 83(21–22), 1792–1803.
Sakurai, S. (2010). "Modeling strategy for jointed rock masses reinforced by rock bolts in tunneling practice." *Acta Geotechnica*, 5(2), 121–126.
Simo, J. C., and Ju, J. (1987). "Strain and stress-based continuum damage models—II. Computational aspects." *Int. J. Solids Struct.*, 23(7), 841–869.
Spada, A., Giambanco, G., and Rizzo, P. (2009). "Damage and plasticity at the interfaces in composite materials and structures." *Comput. Methods Appl. Mech. Eng.*, 198(49–52), 3884–3901.
Taylor, R. L. (2005a). "FEAP—A finite element analysis program version 7.5 user manual."
Taylor, R. L. (2005b). "FEAP—A finite element analysis program version 7.5 programmer manual."
Wang, X., and Liu, X. (2003). "A strain-softening model for steel-concrete bond." *Cem. Concr. Res.*, 33(10), 1669–1673.
Yeih, W., Huang, R., Chang, J. J., and Yang, C. C. (1997). "A pullout test for determining interface properties between rebar and concrete." *Adv. Cem. Based Mater.*, 5(2), 57–65.

J. Eng. Mech. 2011.137:854-861.